ARTICLE

BCL-2 isoform *β* promotes angiogenesis by TRiC-mediated upregulation of VEGF-A in lymphoma

Xiaohang Hang[1,3], Lei Zhao[1,3], Baohong Wu[1,3], Shujun Li[1], Pengpeng Liu[1], Jing Xu[1], Xinyuan Wang[2], Pengliang Chi[1], Chong Chen[1], Ting Niu[1], Lunzhi Dai[2]✉ and Yu Liu[1]✉

Bcl-2 (B-cell lymphoma 2), the first identified anti-apoptosis factor, encodes two transcripts, the long isoform *α* and the short isoform *β*. The current understanding of the Bcl-2 function mainly focuses on Bcl-2α, while little is known about the function of Bcl-2β, which lacks the transmembrane domain and contains 10 unique amino acids at the C-terminus instead. Here, we analyzed the expressions of *BCL-2* two isoforms in diffused large B-cell lymphoma (DLBCL) and found a significant positive correlation between them. Then, with the CRISPR/Cas9-based transcriptional activator (CRISPRa), we generated mouse B-cell lymphomas with *Bcl-2* upregulation from the endogenous locus, in which both *Bcl-2α* and *Bcl-2β* levels were increased. Bcl-2β itself promoted angiogenesis both in vitro and in vivo through increased vascular endothelial growth factor A (VEGF-A). Inhibiting VEGF receptors with Axitinib reduced angiogenesis induced by *Bcl-2β* overexpression. Co-immunoprecipitation and mass spectrometry analysis revealed that Bcl-2β interacted with the T-complex protein ring complex (TRiC). Disruption of TRiC significantly impaired the angiogenesis-promoting activity of Bcl-2β, indicated by reduced VEGF-A protein level and HUVEC tube formation. Thus, our study suggests that *Bcl-2* isoform *β* plays a role in promoting tumor angiogenesis through the Bcl-2β-TRiC-VEGF-A axis.

Oncogene; https://doi.org/10.1038/s41388-022-02372-0

INTRODUCTION

Bcl-2 (B-cell lymphoma 2) is frequently deregulated in many human cancers [1, 2]. It was firstly discovered in B-cell follicular lymphomas with t (14;18) (q32; q21) chromosome translocation, which juxtaposes the *BCL-2* gene under the regulation of IgH transcription enhancer resulting in the overexpression of *BCL-2* [3, 4]. Later, Bcl-2, an inner mitochondria member protein, was identified as a founding member of the Bcl-2 family proteins that block programmed cell death and promote cell survival [5, 6]. Deregulation of *BCL-2* is often associated with a poor prognosis in various cancers. *BCL-2* high expression together with *MYC* overexpression in B-cell non-Hodgkin lymphoma (NHL), named double-hit or double-expressor lymphoma dependent on whether chromosome translocation events are involved or not, is associated with poor prognosis [7]. Compared to more than 80% of human DLBCL who benefited from the current R-CHOP regimen, less than 60% of patients with *BCL-2* and *MYC* overexpression can achieve 5-year survival. Due to the importance of Bcl-2 in cancer development and drug resistance, it became a promising therapeutic target. BH3-mimetics like venetoclax as Bcl-2 inhibitor [8, 9] have been approved for treating patients with chronic lymphatic leukemia or newly diagnosed acute myeloid leukemia, and several clinic studies of combinations with Bcl-2 inhibitors in treating lymphomas are ongoing.

BCL-2 has two isoforms, *BCL-2α* and *BCL-2β* [10]. In most cases, both *BCL-2α* and *BCL-2β* expressions are increased when *BCL-2* is upregulated by translocation or amplification in various cancers. The ratio of *BCL-2β* vs *BCL-2α* is reported higher in chronic myelogenous leukemia [11]. Although Bcl-2α is a well-known anti-apoptotic factor with an oncogenic effect on cancer biology, the Bcl-2β function is still under study. *BCL-2β* shares the exon 1 and exon 2 encoding four BH domains, but lacks exon 3 encoding the transmembrane domain. Besides, Bcl-2β contains unique 10 amino acids (7 amino acids in mouse Bcl-2β) at its C-terminus. Several studies on C-terminal-truncated Bcl-2α showed that the anti-apoptotic role of Bcl-2α relies on the transmembrane domain [12]. Also, adding Bcl-2β with a heterologous transmembrane domain is capable of prolonging cell survival by inhibiting apoptosis. But, *BCL-2α* truncated mutant is not equal to *BCL-2β* due to the lack of Bcl-2β c-terminal 10 amino acids. The role of *BCL-2β* remains elusive.

Here, we investigated the function of Bcl-2β in tumor biology. We first applied a CRISPRa system to upregulate *Bcl-2* gene expression from the endogenous locus to generate murine B-cell lymphoma, in which both *Bcl-2α* and *Bcl-2β* were overexpressed. The further analysis illustrated that Bcl-2β promoted angiogenesis in vitro and in vivo through increased VEGF-A. Our results revealed that *Bcl-2* isoform *β* plays a role in tumor angiogenesis.

RESULTS

BCL-2β is frequently upregulated in human B-cell lymphomas

BCL-2 is overexpressed frequently in B-cell lymphomas and is often associated with poor prognosis. To investigate the

[1]Department of Hematology, State Key Laboratory of Biotherapy and Cancer Center, West China Hospital, Sichuan University, Chengdu, Sichuan, China. [2]Department of General Practice and National Clinical Research Center for Geriatrics, State Key Laboratory of Biotherapy, West China Hospital, Sichuan University, Chengdu, Sichuan, China. [3]These authors contributed equally: Xiaohang Hang, Lei Zhao, Baohong Wu. ✉email: lunzhi.dai@scu.edu.cn; yuliuscu@scu.edu.cn

Received: 23 January 2022 Revised: 25 May 2022 Accepted: 30 May 2022
Published online: 14 June 2022

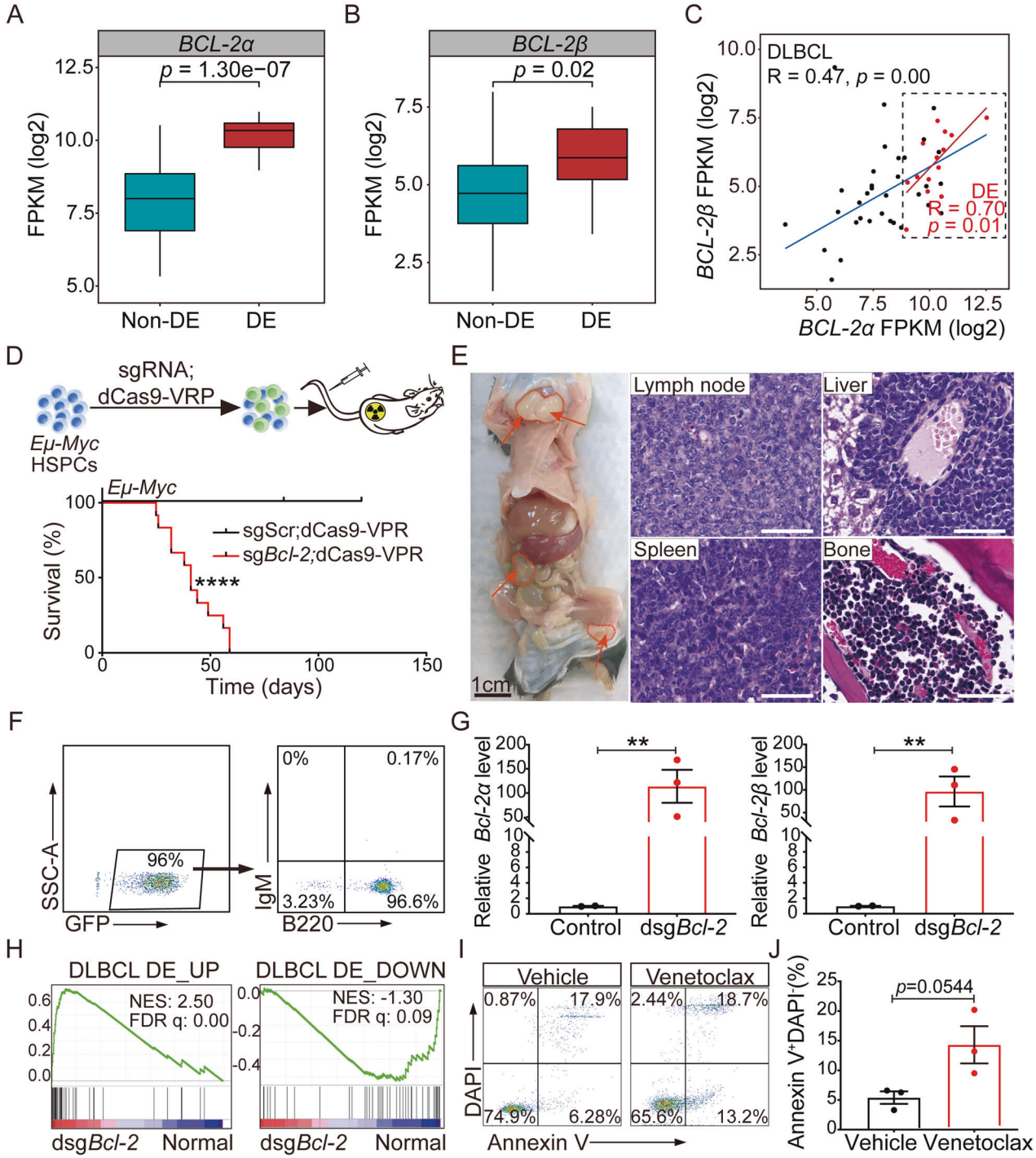

expression of *BCL-2* two mRNA variants, *BCL-2α* and *BCL-2β*, we analyzed the RNA-seq data from the TCGA-DLBC cohort with a total of 48 patients (Fig. 1A, B, Supplementary Fig. 1). *BCL-2* overexpression highly co-occurs with *MYC* overexpression in B-cell lymphoma. Therefore, we selected the patients with both *MYC* and *BCL-2* high-expression (top 50%) as double expressor (DE), and found that the *BCL-2β* expression level is even higher in DE (Fig. 1B). The expression of *BCL-2β* is significantly positively correlated with that of *BCL-2α* in all patients ($R = 0.47$, $p = 0.00073$), and this correlation was stronger in DE patients ($R = 0.7$, $p = 0.0056$) (Fig. 1C).

Mimicking *BCL-2β* upregulation in mouse lymphoma with CRISPRa

Next, we applied the CRISPRa system, a catalytically dead Cas9 fused to multiple transcription activators (dCas9-VP64-p65-Rta, dCas9-VPR) [13], to generate a mouse B-cell lymphoma model with the endogenous mouse *Bcl-2* gene upregulation to mimic DEL patients, in which both *BCL-2α* and *BCL-2β* transcripts were increased. We first chose 12 sgRNAs targeting the promoter region of *Bcl-2* to examine the effect of the CRISPRa system (Supplementary Fig. 2). The fewest and most efficient combination of *Bcl-2* sgRNAs were sgRNAs targeting −97, −217, and −993, which were

Fig. 1 Modeling double expressor lymphoma-associated *Bcl-2β* upregulation with CRISPRa in mice. The mRNA levels of *BCL-2α* (**A**) and *BCL-2β* (**B**) in non-DE and DE lymphomas from the TCGA-DLBC cohort, $n = 14$ for DE and $n = 34$ for Non-DE (DE, defined by high expression both of *MYC* and *BCL-2* through median RNA expression level; Non-DE, other DLBCL patients except DE). **C** The correlation of *BCL-2α* and *BCL-2β* expression in DLBCL patients, $R = 0.47$, $p = 0.00073$ (all black and red points), and in DE patients, $R = 0.7$, $p = 0.0056$ (red points in Dotted box). **D** Top: schematic of mouse *Myc*-driven B-cell lymphoma generated by transplantation. *Eμ-Myc* E13.5 HSPCs were transduced with CRISPR/dCas9-VPR and transplanted into sub-lethally irradiated recipient mice. Bottom: Kaplan–Meier tumor-free survival curve of recipient mice, $n = 11$ for the sgScr group and $n = 12$ for the sg*Bcl-2* group. ****$p < 0.0001$ (log-rank test). **E** Left: Representative anatomic photograph of sg*Bcl-2*; dCas9-VPR recipient mice. Scale bar,1 cm. Middle and right Representative H&E stating picture showing enlarged lymph nodes, liver, spleen, and bone in *Eμ-Myc*; sg*Bcl-2*; dCas9-VPR recipient mice. scale bar, 50 μm. **F** Representative flow plots showing the expression of GFP, B220, and IgM of harvested sg*Bcl-2*; dCas9-VPR lymphoma cells. **G** Relative mRNA levels of *Bcl-2α* and *Bcl-2β* in sg*Bcl-2;* dCas9-VPR lymphoma cells, measured by RT-PCR, $n = 2$ for control group and $n = 3$ for dsg*Bcl-2* group. Error bar represents Mean with SEM. **$p < 0.01$ (unpaired two-tailed *t*-test). **H** Gene Set Enrichment Analysis (GSEA) showing the enrichments of gene signatures (top 200 differential expression genes of upregulation or downregulation) of DE with dsg*Bcl-2* lymphomas compared to normal lymph nodes (UP: NES = 2.50; FDR $q = 0.00$; DOWN: NES = −1.30; FDR $q = 0.09$). **I** Representative flow cytometry results of Annexin V staining results of dsg*Bcl-2* lymphoma cells harvested from 2nd transplanted mouse bone marrow after ABT-199 or vehicle treatment. **J** The histogram shows the percentage of Annexin V^+ $DAPI^-$ lymphoma cells quantitated from I $n = 3$ recipient mice for each group. Error bar represents Mean with SEM, $p = 0.0544$ (unpaired two-tailed *t*-test).

then cloned into one retrovirus-based vector (Supplementary Figs. 2 and 3). Hematopoietic stem and progenitor cells (HSPCs) from *Eμ-Myc* mice [14] were transduced with dCas9-VPR and sgRNAs for *Bcl-2*(sg*Bcl-2*) or scramble (sgScr) and then injected into sub-lethally irradiated wild-type C57BL/6 recipient mice. Lymphoma development was monitored by palpation twice per week. Recipient mice transplanted with *Eμ-Myc*; sg*Bcl-2*; dCas9-VPR HSPCs developed lymphoma very fast (median onset 41 days, $p < 0.01$), while control mice with sgScr were healthy with no lymphoma detected in observed time (>80 days after transplantation) (Fig. 1D).

The resulting *Eμ-Myc*; sg*Bcl-2*; dCas9-VPR (named dsg*Bcl-2*) lymphomas were enriched in enlarged lymph nodes (Fig. 1E). These lymphoma cells were very aggressive and infiltrated into multiple organs including the liver, spleen, and bone as shown by hematoxylin and eosin (H&E) staining, consistent with other *Eμ-Myc* lymphomas reported before [14] (Fig. 1E). Flow cytometry analysis results showed that resulting dsg*Bcl-2* lymphoma cells are GFP^+ and $B220^+IgM^-$, indicating that they originated from donor B progenitor cells with sg*Bcl-2*; dCas9-VPR (Fig. 1F). Then, we analyzed the *Bcl-2* expression status by RT-PCR, and found that both *Bcl-2α* and *Bcl-2β* transcripts were dramatically increased in the dsg*Bcl-2* lymphoma cells, compared to control *Eμ-Myc* lymphoma cells (Fig. 1G).

To investigate whether our dsg*Bcl-2* lymphoma model recapitulated the molecular signature of human DLBCL with *MYC* and *BCL-2* double high-expression (DLBCL_DE), we performed RNA-seq analysis of dsg*Bcl-2* lymphoma cells. The gene set enrichment analysis (GSEA) showed that the upregulated genes in dsg*Bcl-2* model were significantly positively enriched in DLBCL_DE, so did downregulate genes in normal lymph nodes (Fig. 1H). We also examined the drug response of the dsg*Bcl-2* lymphoma cells to Bcl-2 inhibitor venetoclax (ABT-199) in vivo (Fig. 1I). Compared to the vehicle group, GFP^+ dsg*Bcl-2* lymphoma cells had a higher rate of apoptotic cells (Annexin V^+DAPI^-) (Fig. 1J), consistent with the previous report [15]. These results indicated that the dsg*Bcl-2* lymphoma mouse model we constructed well mimicked the patients with double expressor lymphoma.

Bcl-2β promotes angiogenesis

Bcl-2α is a well-known oncogene to drive B-cell lymphoma. To investigate whether *Bcl-2β* also plays a role in lymphoma biology, we cloned the *Bcl-2β* cDNA and introduced it into *Eμ-Myc* HSPCs to examine its role in driving lymphomagenesis. However, the *Bcl-2β* overexpressed group did not show a significant advantage in lymphomagenesis (Supplementary Fig. 4). It has been reported that *Bcl-2β* overexpression could transform NIH3T3 cells into tumors in vivo [16]. Therefore, *Bcl-2β* cDNA was transduced into NIH3T3 cells and subcutaneously injected into recipient nude mice, and monitored the tumor growth. Compared to the control group, NIH3T3 cells with *Bcl-2β* overexpression grew significantly faster and 8/8 (100%) transformed into the tumor with malignant growth (Fig. 2A and Supplementary Fig. 5A, B). *Bcl-2β* overexpression in harvested tumors was confirmed by red fluorescence detected in tumors (Supplementary Fig. 5C), dramatical upregulation of *Bcl-2β* expression, and increased Bcl-2β protein level (Fig. 2B. C).

Interestingly, we noticed that *Bcl-2β*-overexpressed tumors were darker than controls (Supplementary Fig. 5A), suggesting that more vessels were generated in *Bcl-2β*-overexpressed tumors. The H&E staining results confirmed that more red blood cells infiltrated into *Bcl-2β*-overexpressed tumors than that in controls (Fig. 2D). Consistently, more microvessels were observed in *Bcl-2β*-overexpressed tumors as shown by the endothelial marker CD31 staining (Fig. 2D). To investigate the role of *Bcl-2β* in vessel formation, we applied the endothelial cell tube formation assay using human umbilical vein endothelial cells (HUVEC). Media collected from NIH3T3 cells carrying *Bcl-2β* cDNA or empty vector were added into HUVEC. After 7 h incubation, we found that more tubes were formed within the media from *Bcl-2β* overexpressed NIH3T3 cells than that from control cells (Fig. 2E), in which tube number, junction number, total length, and total branching length were dramatically and significantly increased (Fig. 2F).

As *Bcl-2α* was reported to play a role in promoting angiogenesis [17], we generated *Bcl-2* knockout NIH3T3 cell lines with CRISPR/Cas9 technology to exclude the influence of endogenous *Bcl-2α* (Supplementary Fig, 6A–C). In these *Bcl-2* knockout 3T3 cells, no Bcl-2 protein was detected as shown in the Western blotting result (Fig. 3A). Then, we transduced $Bcl\text{-}2^{-/-}$ 3T3 cells with *Bcl-2β* cDNA or empty vector, followed by performing the tube formation assay. Results showed that without endogenous *Bcl-2*, exogenous *Bcl-2β* expression accelerated the HUVEC tube formation with significantly more tubes and branchings, more nodes, and junctions (Fig. 3B, C). We also examined venetoclax role in the *Bcl-2β*-induced HUVEC tube formation, and found little effect with venetoclax treatment (Supplementary Fig. 7). Taken together, these results supported that dysregulated *Bcl-2β* contributes to tumor angiogenesis, which can not be repressed by venetoclax.

Vascular endothelial growth factor A (VEGF-A) is a prominent factor in promoting new blood vessel formation. To test whether VEGF-A is involved in *Bcl-2β*-induced angiogenesis, we examined VEGF-A expression in the $Bcl\text{-}2^{-/-}$ NIH3T3 cells with *Bcl-2β* cDNA or empty vector. The mRNA levels of *VEGFA* have slight changes in cells with or without *Bcl-2β* cDNA (data not shown). However, both cellular and secreted VEGF-A protein are increased in *Bcl-2β*-overexpressed cells (Fig. 3D). With VEGF-A receptors inhibitor Axitinib treatment, *Bcl-2β*-driven tube formation was repressed

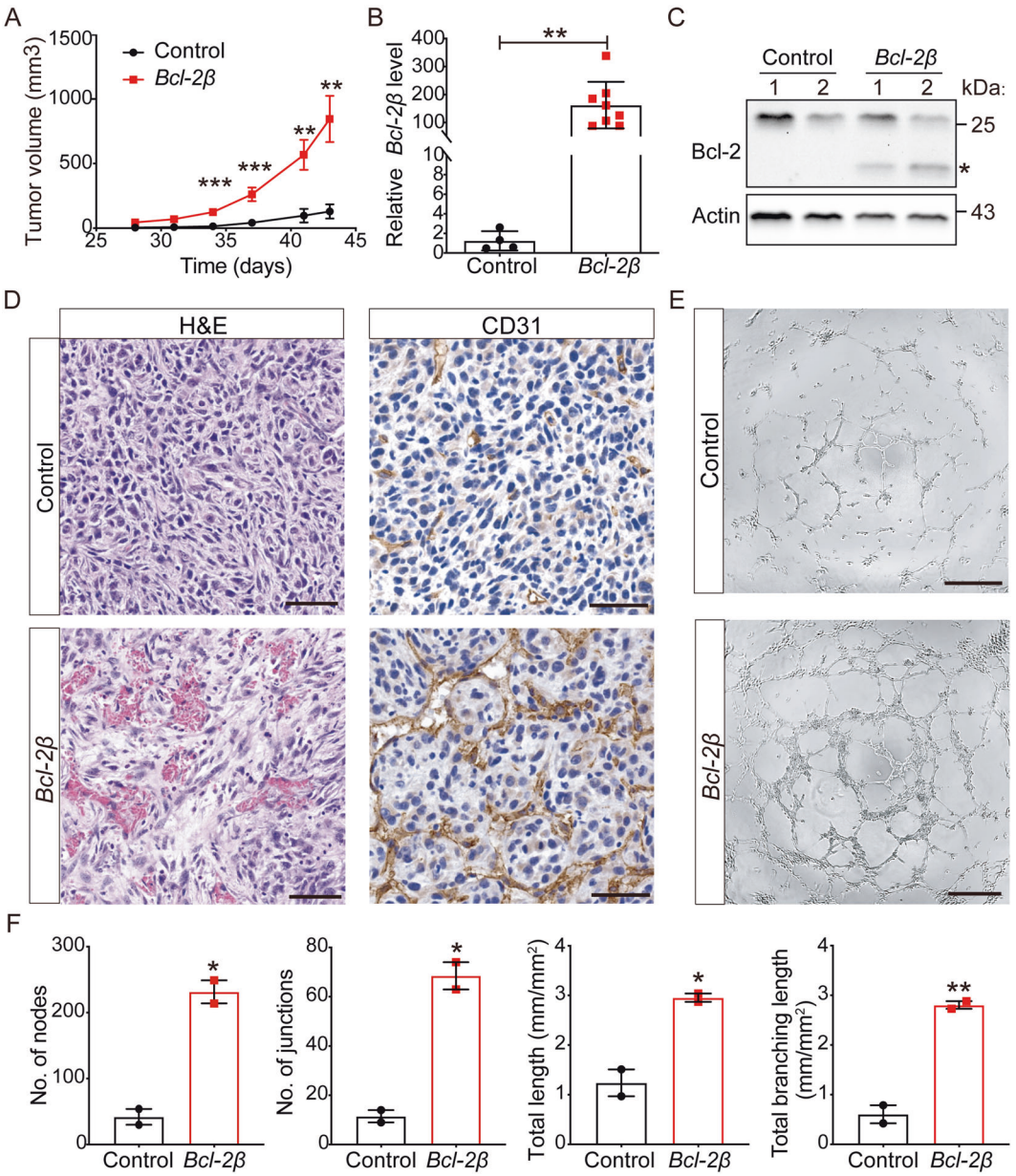

Fig. 2 ***Bcl-2β* promotes tumorigenesis and angiogenesis. A** Tumor growth curve of NIH3T3 cells transduced with empty vector (Control) or *Bcl-2β* cDNA (*Bcl-2β*) in nude mice subcutaneously, $n = 8$ for each group. **B** Relative mRNA levels of *Bcl-2β* in tumors harvested from A. **C** Representative Western blots showing Bcl-2β in tumor cells from A. The asterisk indicates the protein band of Bcl-2β. **D** Representative images of H&E staining and immunohistochemical staining of CD31 for Control or *Bcl-2β* tumors. Scale bar, 50 μm. **E** Representative images of HUVEC tube formation under the medium from NIH3T3 cells transduced with empty vector (Control) or *Bcl-2β* cDNA (*Bcl-2β*). Scale bar: 500μm. **F** The number of nodes, junctions, total length, and total branching length of HUVEC tubes in E was quantitated by ImageJ, $n = 2$ for each group. Error bar: mean with SEM. *$p < 0.05$, **$p < 0.01$, ***$p < 0.001$ (unpaired two-tailed *t*-test).

(Fig. 3E, F). These results suggested that *Bcl-2β* promotes new blood vessel formation through VEGF-A.

Co-IP mass spectrometry reveals the interaction of Bcl-2β and TRiC

Unlike *Bcl-2α* located on the outer mitochondria membrane, *Bcl-2β* was mainly in the cytosol, as shown by immunofluorescence staining with mitochondria marker MitoTracker (Supplementary Fig. 8A). Thus, it was not a surprise when we found that overexpressed *Bcl-2β* had little impact on cell apoptosis (Supplementary Fig. 8B). To explore the molecular mechanisms of Bcl-2β regulating VEGF-A, we performed co-immunoprecipitation (co-IP) and mass spectrometry (MS) with anti-FLAG antibody to pull down FLAG-tagged Bcl-2β. Multiple components in the T-complex protein Ring Complex (TRiC) (CCT2, CCT8, CCT5, TCP1, CCT4, and CCT7) were successfully co-immunoprecipitated with Bcl-2β (Fig. 4A, B). co-IP and Western blotting results confirmed the interaction between Bcl-2β and CCT2, CCT5 or CCT8 (Fig. 4C).

TRiC is required for *Bcl-2β*-induced angiogenesis

Further, we analyzed the impact of TRiC on *Bcl-2β*-driven angiogenesis. We constructed sgRNAs to target components in TRiC including *Tcp1*, *Cct2*, *Cct4*, *Cct5*, *Cct7*, or *Cct8*, and measured the efficiency of these sgRNAs by T7E1 assay (Supplementary Fig. 9). With these sgRNAs, VEGF-A protein levels in *Bcl-2β*-over-expressed NIH3T3 cells were dramatically reduced, compared to

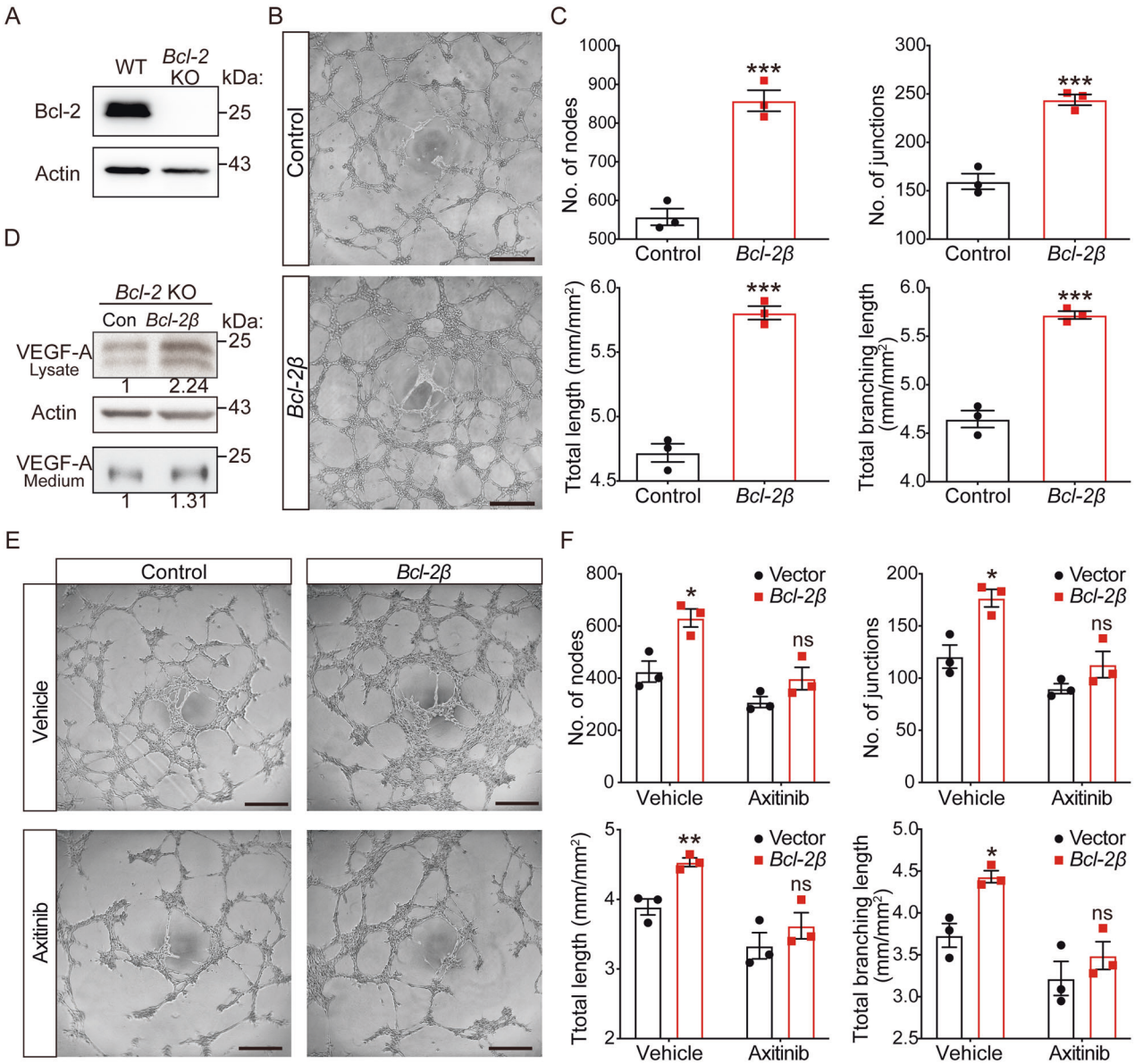

Fig. 3 *Bcl-2β* promotes angiogenesis through increased VEGF-A secretion. A Western blotting results of Bcl-2 in *Bcl-2* wild-type (WT) or knockout (KO) NIH3T3 cells. **B** Representative images of HUVEC tube formation with the medium harvested from *Bcl-2*$^{-/-}$ NIH3T3 cells transduced with empty vector (Control) or *Bcl-2β* cDNA (*Bcl-2β*). Scale bar: 500 μm. **C**. The number of nodes, junctions, total length, and total branching length of HUVEC tubes in **B** was quantitated by ImageJ. **D** Western blotting results of VEGF-A (both in lysates and medium) when *Bcl-2β* overexpressed or not in *Bcl-2*$^{-/-}$ NIH3T3 cells. **E** Representative images of HUVEC tube formation with the medium harvested from *Bcl-2β* overexpressed (control: empty vector) in *Bcl-2*$^{-/-}$ NIH3T3 cells treated with vehicle or Axitinib. Scale bar: 500 μm. **F** The number of nodes, junctions, total length, and total branching length of HUVEC tubes in **E** was quantitated by ImageJ, $n = 3$ for each group. The error bar represents mean with SEM. ns not significant, *$p < 0.05$, **$p < 0.01$, ***$p < 0.001$ (unpaired two-tailed *t*-test).

scramble sgRNA (Fig. 4D). Consistently, media collected from these cells has much less effect on promoting HUVEC tube formation (Fig. 4E, F). Together, these results suggested that *Bcl-2β* overexpression induced new blood vessel formation probably through the TRiC/VEGF-A axis.

To study the clinic relevance of our finding, we analyzed the TCGA-DLBCL RNA-seq data and found that VEGF-A related pathways such as "ABE_VEGFA_TARGETS", "HALLMARK_ANGIOGENESIS" were enriched in *BCL-2β* high group, determined by median RNA level of *BCL-2β* (Fig. 5A). *VEGFA* gene expression was significantly upregulated in *BCL-2β* high group but not in *BCL-2α* high group (Fig. 5B). Furthermore, the expression of genes encoding TRiC component *Cct2*, *Cct5*, or *Cct8* were positively correlated with *VEGFA* and VEGFA_target mRNA levels (Fig. 5C). We also analyzed the clinical samples from Non-DEL or DEL patients collected from West China Hospital. The immunohistochemical staining results with anti-CD31 antibody showed more blood vessels formed in DEL samples (Fig. 5D). Altogether, these results supported that *BCL-2β* contributed to lymphoma angiogenesis.

Overall, our findings suggested that *Bcl-2β*, one of the *Bcl-2* isoforms, could upregulate VEGF-A protein levels and promote angiogenesis through the T-complex protein Ring Complex (Fig. 6).

DISCUSSION

BCL-2 upregulation is common in various human cancers, especially in double-expressor lymphoma. The role of *BCL-2* in tumor biology has long been considered as that of its long isoform

A

Protein ID	Unique Peptides	AAs	kDa.	Score.
CCT2	20	535	57.44	69.47
CCT8	17	548	59.52	48.54
CCT5	14	541	59.59	43.85
TCP1	12	556	60.41	34.05
CCT4	10	539	58.03	25.39
Bcl-2	9	236	26.39	192.59
CCT7	9	544	59.61	24.10

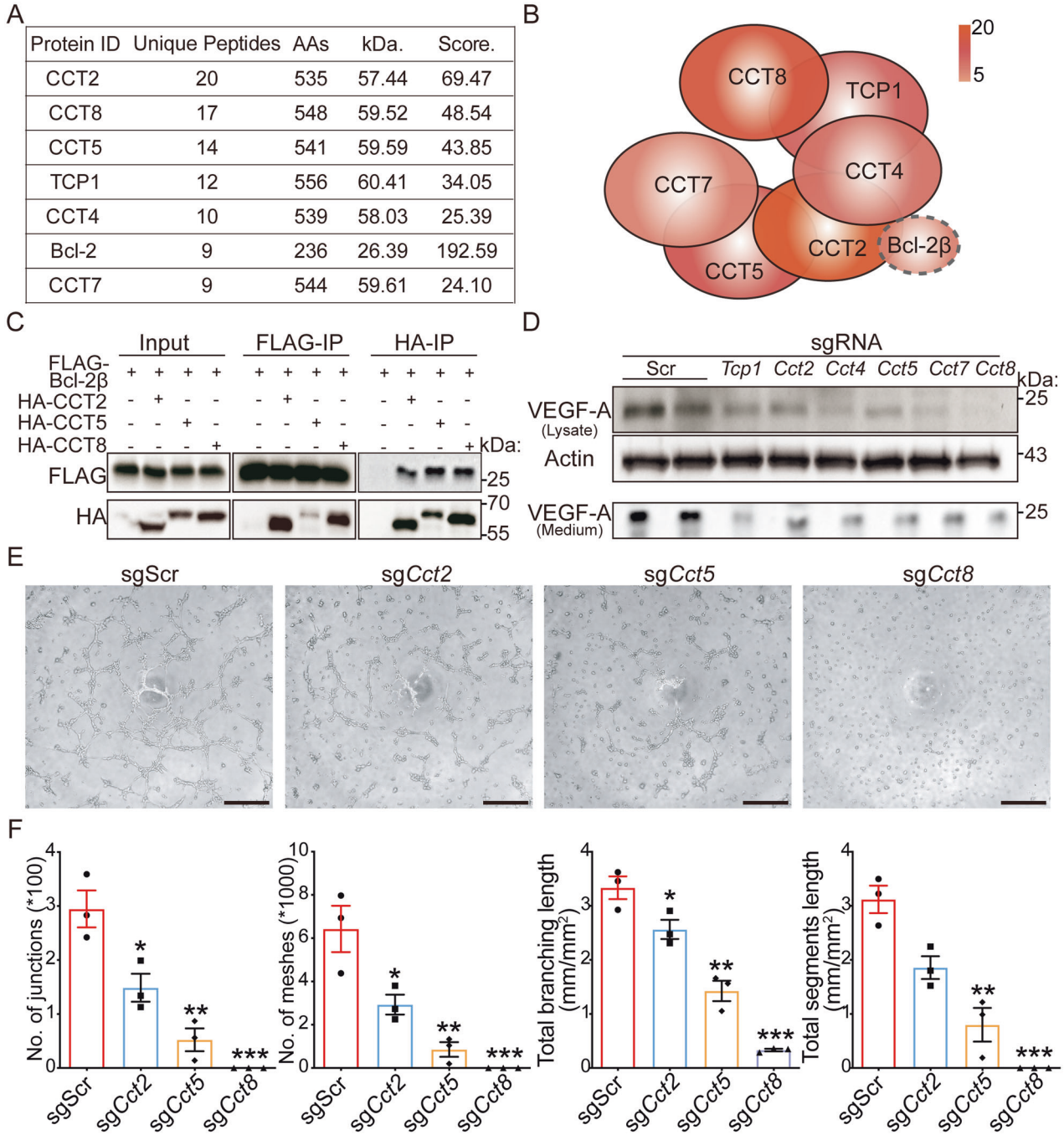

Fig. 4 Bcl-2β interacts with the TRiC, which is essential for angiogenesis. A Summary of co-IP and MS results that the TRiC components pulled down by FLAG-Bcl-2β. Protein ID (UniprotKB protein description), Unique peptides (The number of peptide sequences unique to a protein group), MW (molecular weight), Score (The sum of the scores of the individual peptides). **B** Schematic diagram represents A. Colors indicated the Mascot scores of each component measured in **A**. **C** co-IP and Western blotting results show the interaction between Bcl-2β and CCT2, CCT5, or CCT8. **D** The intracellular (lysate) and extracellular (medium level of VEGF-A protein in *Bcl-2β* overexpressed cells carrying various sgRNAs. **E**. Representative images of HUVEC tube formation with the medium from *Bcl-2β* overexpressed cells with sgRNA targeting scramble or TRiC subunits. Scale bar: 500μm. **F**. The number of junctions, the number of meshes, the total branching length, and the total segments length of HUVEC tubes in **E** were quantitated by ImageJ, $n = 3$ for each group. Error bar represents mean with SEM, $^{*}p < 0.05$, $^{**}p < 0.01$, $^{***}p < 0.001$ (unpaired two-tailed *t*-test).

BCL-2α. In contrast, there is little study on *BCL-2* short isoform, *BCL-2β*. Here, we find that overexpression of *BCL-2β* could induce tumor angiogenesis. Further, we show that Bcl-2β interacted with chaperonin T-complex protein Ring Complex, which is required for vascular endothelial growth factor VEGF-A protein secretion and vessel tube formation. These results suggest that *BCL-2* upregulation, which frequently happens in cancers and is associated with poor prognosis, might have an impact on cancer biology through both α and β isoforms.

Although Bcl-2α is a well-studied anti-apoptotic factor, the role of Bcl-2β in cellular apoptosis is unclear. Our apoptosis assay suggests that *Bcl-2β* may not contribute to cellular apoptosis. Compared to Bcl-2α, Bcl-2β contains the same N-terminus and four Bcl-2 homologies (BH) domains as Bcl-2α but does not have

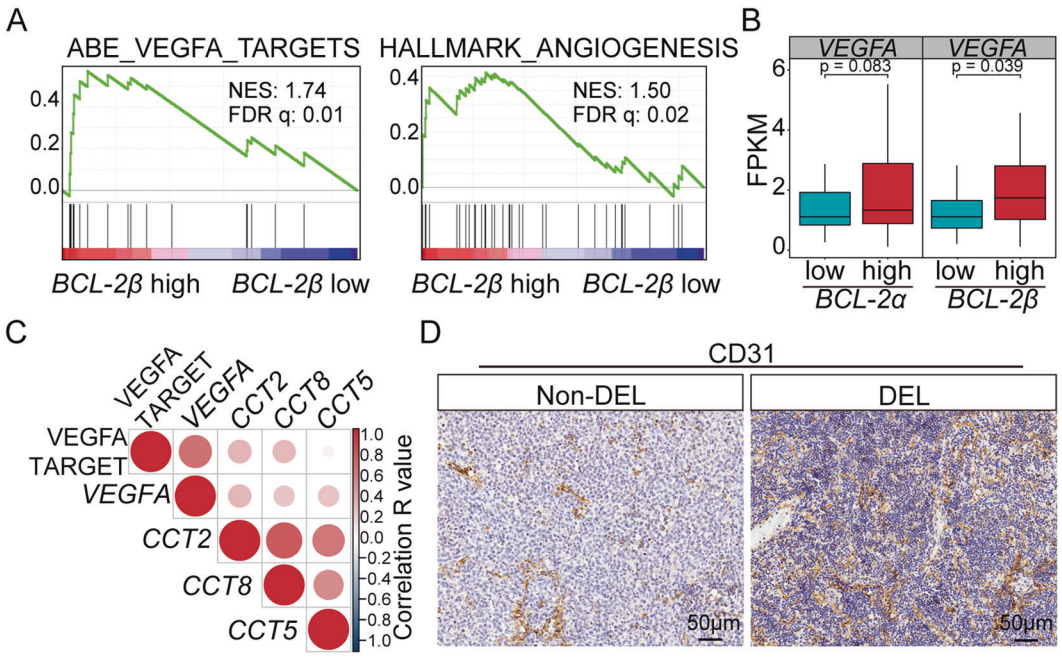

Fig. 5 The correlation of the expression levels of *BCL-2β* and TRiC components with angiogenesis in human DLBCL. A GSEA shows the enrichment of the "ABE_VEGFA_TARGETS" (NES = 1.74; FDR $q = 0.01$) and "HALLMARK_ANGIOGENESIS" (NES = 1.50; FDR $q = 0.02$) pathways in *BCL-2β* high expressed group compared with a low expressed group (separated by *BCL-2β* median RNA level, $n = 24$ for each group). **B** Relative expression levels of *VEGFA* in *BCL-2α/ BCL-2β* high expression group and low expression group in DLBCL patients, n = 24 for each group (*BCL-2α/BCL-2β* high and low, separated by median RNA level, $n = 24$ for each group). **C** Pearson correlation matrix for *VEGFA*, VEGFA TARGET, and *CCT2, CCT5, CCT8* based on TCGA-DLBC cohort, $n = 48$. **D** Immunohistochemical staining images of CD31 for lymphoma from Non-DEL or DEL patients. Scale bar, 50 μm.

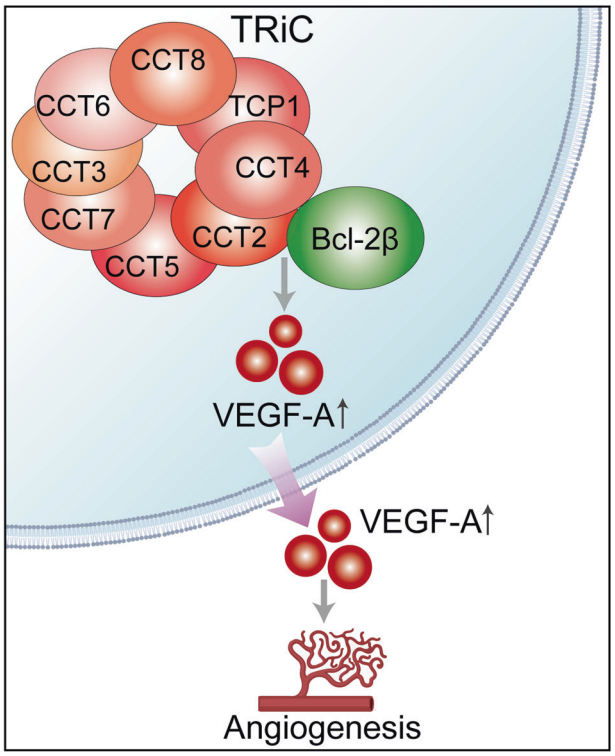

Fig. 6 Schematic illustration of Bcl-2β-TRiC-VEGF-A working model. Bcl-2β overexpression promotes tumor angiogenesis through interacting with TRiC, which is required for VEGF-A increase and secretion.

the transmembrane (TM) domain and contains unique 10 amino acids at C-terminus instead. The transmembrane domain is required for Bcl-2α located on the outer mitochondria membrane. Some studies of TM-truncated Bcl-2α mutants indicate that TM is important for Bcl-2α function including locating organelles [18] and regulating apoptosis [19]. However, other studies suggest that TM is not required for the Bcl-2α anti-apoptosis effect [20, 21]. Of note, TM-truncated Bcl-2α mutant is not the same as Bcl-2β which has a C-terminal 10-amino acid stretch. Whether and how the C-terminus of Bcl-2β would contribute to its function in lymphoma need further studies.

The relationship between *BCL-2* and *VEGFA* has been studied in various cancer cells. It has been reported that *BCL-2α* can upregulate *VEGFA* gene expression through HIF-1 in human melanoma cells and breast carcinoma cells [17, 22]. Exogenous *VEGFA* treatment-induced *BCL-2* expression in human dermal microvascular endothelial cells [23] and leukemia [24]. Our finding extends the understanding of the crosstalk between *BCL-2* and *VEGFA* that *BCL-2β* can induce angiogenesis through the TRiC-VEGF-A axis. Chaperones like Hsp90, Glypican-1, and αB-crystallin have been reported to contribute to VEGF-A folding or misfolded VEGF-A returning to ER and re-folding [25–28]. TRiC, as an essential eukaryotic cellular chaperonin, may help VEGF-A in a similar way as other chaperones. Given the general upregulation of Bcl-2 in human cancers, it would be interesting to explore whether Bcl-2β has common functions in various types of malignancies other than lymphoma.

METHODS

Cell culture

HEK293T (RRID: CVCL_0063), NIH3T3 (ATCC Cat# CRL-1658, RRID: CVCL_0594), and HUVEC (ATCC Cat# CRL-1730, RRID: CVCL_2959) were from ATCC, and

cultured at 37 °C in DMEM medium (Gibco #C11995500BT) supplemented with 10% (v/v) fetal bovine serum (FBS, Gibco #10099141) and 1% (v/v) penicillin (100 U/ml)/streptomycin(0.1 mg/ml) (Gibco #15140122). 10 μM venetoclax or DMSO was added into NIH3T3 culturing medium for 24 h. 1 μM VEGFR inhibitor Axitinib (Selleck Chemicals Cat#S1005) was used to treat Human Umbilical Vein Endothelial Cells (HUVEC) cells in tube formation assay.

Mice

All mice experiments were approved by the Institutional Animal Care and Use Committees of Sichuan University. *Eμ-Myc* transgenic mice (RRID: IMSR_JAX:002728) were from Jackson Laboratories. Hematopoietic stem cells and progenitor cells (HSPCs) of *Eμ-Myc* were isolated from mice embryos at 14.5 days. To generate murine B-cell lymphoma, *Eμ-Myc* HSPCs were transduced with retroviruses and intravenously injected (i.v.) into sub-lethally irradiated (4.5Gray) C57BL/6 recipient mice (6–7weeks old, female). All recipient mice were divided into each group randomly before transplantation and monitored twice per week by palpation. The immunophenotypes of mouse lymphoma cells were analyzed by flow cytometry with antibodies purchased from Biolegend. Statistical analysis of mice tumor-free survival curve was accomplished with the log-rank test from Prism 9. Mouse lymphoma model treated with Bcl-2 inhibitor venetoclax (ABT-199, Selleck Chemicals #S8048) were used to treat mice as previously described [15]. Briefly, venetoclax, dissolved in 10% ethanol, 40% PEG 400, and 50% oil, was delivered to lymphoma-bearing mice (16 days after transplanted with 10^6 lymphoma cells) once a day for 3 consecutive days by gavage at the dosage of 50 mg/kg. One day after the last drug treatment, lymphoma cells were harvested from recipient mice with enlarged lymph nodes and analyzed by Annexin V staining.

Annexin V staining

The cells required for apoptosis analysis were collected by centrifugation at 1500 rpm for 3 min. After washing with PBS buffer, FITC-labeled AnnexinV (Biolegend Cat#640914) antibody and nucleic acid dye DAP were used for staining. The proportion of apoptotic cells was analyzed by flow cytometry (BD Biosciences LSRFortessa).

CRISPR-activation system

The CRISPRa system used here was CRISPR-dCas9-VPR [29], which has a retrovirus-based backbone as pMSCV-dCas9-VP64-p65-Rta. Another element of the system, sgRNA, uses modified (Cas9 was replaced with the mCherry fluorescent protein) lentiCRISPR V2 (RRID:Addgene_52961) plasmid as the backbone. sgRNAs (listed in supplementary table) were designed for targeting the various promoter region (2 kb upstream of the transcription start site) of *Bcl-2* (from DNA2.0 Gene Design & Synthesis – ATUM website, Supplementary Fig. 1A). The efficiency of these sgRNA combinations in upregulating *Bcl-2* gene expression was examined in NIH3T3 cells (Supplementary Fig. 1B). Three *Bcl-2* sgRNAs were cloned at one step into a lentivirus-based vector (named sg*Bcl-2*, Supplementary Fig. 2A, B). The strategy of cloning multiple sgRNAs in one step is to use the characteristics of the restriction endonuclease DraIII (New England BioLabs Cat#R3510S). Virus packaging and infection were done as previously described [30, 31].

cDNA cloning

Bcl-2α, *Bcl-2β*, and C-terminal-truncated Bcl-2β cDNA sequences were obtained from the cDNA library of pre-B cells, digested by BglII (Cat#R0144S) and EcoRI (Cat#R0101S) endonuclease from New England BioLabs, and followed by cloning into the retroviral plasmid MSCV-cDNA-IRES-GFP/mCherry. 3xFLAG-tagged *Bcl-2α* and *Bcl-2β* cDNA were cloned into retroviral plasmid MSCV-IRES-GFP, HA-tagged *Cct2, Cct5, Cct8* cDNA were cloned into retroviral plasmid MSCV-IRES-mCherry.

RT-qPCR

Total RNA was extracted by Trizol (Thermo Fisher Scientific #15596026), according to the manufacturer's protocol, followed by reverse transcription with HiScript-III RT SuperMix kit (Vazyme Cat#R323-01). qPCR was performed with Fast SYBR Green Mastermix (Vazyme Cat#Q711-02/03) on the StepOne Real-Time PCR System (Thermo Fisher Scientific, Applied Biosystems QuantStudio 3).

Immunohistochemistry

Paraffin-embedded tissues were sectioned into 5 μm (Leica RM2125 RTS Manual Microtome, RRID:SCR_018040). Hematoxylin-eosin (Sigma Cat#318906) staining was performed according to the manufacturer's protocol. Immunohistochemical staining of anti-CD31(Servicebio Cat#GB11063-1) had been done as the protocol described. Images were collected by microscope slide scanner (PANNORAMIC MIDI, 3DHISTECH) and analyzed by CaseViewer (RRID: SCR_017654).

Western blotting

Whole cell lysate was extracted with cell lysis buffer (Cell Signaling Technology, Cat#9803), according to the manufacturer's protocol. Proteins in lysate were resolved by 12% SDS/PAGE and then transferred onto PVDF membranes. Bcl-2 (Abcam Cat# ab182858, RRID: AB_2715467), VEGF-A (Abcam Cat# ab46154, RRID: AB_2212642), Actin (Invitrogen, beta-actin-HRP RK241732) antibodies were used for western blotting.

Co-immunoprecipitation and mass spectrometry

3xFLAG-tagged *Bcl-2α* and *Bcl-2β* cDNA, HA-tagged *Cct2, Cct5, Cct8* cDNA were transduced into NIH3T3 cells. Whole-cell lysates were extracted from 10^7 NIH3T3 cells with RIPA lysis buffer (50 mM Tris-pH 7.4, 150 mM NaCl, 1% NP-40, 0.5% sodium deoxycholate) supplemented with protease inhibitor cocktail (Roche #4693159001) and incubated with anti-FLAG M2 mAb-conjugated agarose beads (Sigma-Aldrich Cat# A2220, RRID: AB_10063035) or anti-HA antibody (Cat# 3724, RRID: AB_1549585). Then the protein samples prepared by co-immunoprecipitation were processed and analyzed by the q-EXactive Plus instrument (Thermo Scientific Cat#IQLAAEGAAPFALGMBDK). The horseradish peroxidase (HRP)-conjugated FLAG antibody was purchased from Sigma (Sigma-Aldrich Cat# A8592, RRID: AB_439702). The anti-HA antibody was from Cell signaling technology (Cat# 3724, RRID: AB_1549585) for Co-IP and western blotting.

Tube formation assay

Tubule formation experiment was performed as previously described [32]. About 0.4 million NIH3T3 cells transfected with empty vector or *Bcl-2β* cDNA were plated in one well of the six-well plate. Cell culture medium from untreated, vehicle (0.1%DMSO) treated or 10 μM venetoclax treated NIH3T3 cells, were collected 24 hours later to culture HUVEC. The HUVEC were plated in Matrigel (Corning #356237)-coated 96-well plates as 10000 cells per well. In VEGFR inhibitor trials, 0.1% DMSO (vehicle) or 1 μM of Axitinib was added into the collected medium for treating HUVEC. The tube formation was visualized by microscope (Olympus IX73), and images were analyzed by ImageJ. The number of nodes, junctions, total length, and branching length was analyzed by the Angiogenesis Analyzer plug-in for ImageJ.

RNA sequencing and analysis

Lymphoma cells harvested from enlarged lymph nodes of lymphoma-bearing mice were used for RNA sequencing. Total RNA was extracted with Trizol reagent. RNA was analyzed by the Agilent Technologies 2100 bioanalyzer. Libraries were prepared by the BGI company, and sequencing was performed by the BGIseq500. The RNA-seq reads were aligned to the reference genome (mm10) by STAR [33]. DESeq2 [34] was used to normalize the transcripts and perform the differential expression analysis. The genes with log2-fold change ≥ 1 or ≤ -1; p value < 0.05 were selected as significantly differentially expressed genes. Gene set enrichment analysis (GSEA) [35] was performed to analyze the similarity between CRISPRa mouse lymphomas and human DLBCL from TCGA-DLBC with both *BCL-2* and *MYC* high expressions. The RNA-seq data of mouse and human normal lymph nodes used in GSEA analyses were from GEO datasets GSE132899 (mouse) and GSE157671 (human), respectively. Differentially expressed genes for pathway enrichment analysis were also performed by GSEA.

All patients with diffuse large B-cell lymphoma in this study were from the TCGA-DLBC cohort. DE was defined according to those with both *BCL-2* and *MYC* expressions above the median level. The correlation of *BCL-2α* and *BCL-2β* in DLBCL and DE patients was visualized by ggplot2. DLBCL patients with high or low expression levels of *BCL-2β*, *BCL-2α*, or TRiC were also divided into groups according to the median expression levels. The correlation network of VEGF-A, VEGF-A target signature (GSEA: RAFFEL_VEGFA_TARGETS_UP), and TRiC components was constructed by Corrplot [36].

Human samples

Paraffin-embedded lymphoma sections of patients with diffuse large B cell lymphoma or double expressor lymphoma for immunohistochemical staining were obtained from West China Hospital, Sichuan University, China. The diagnosis followed the 2016 WHO tumor classification. The study was

approved by Biomedical Ethics Committee, West China Hospital, Sichuan University (2019-114), and all sections were collected with informed consent.

Statistical analysis

Statistical analysis was performed by GraphPad Prism9 (RRID: SCR_002798). Kaplan–Meier tumor-free survival were analyzed by log-rank test. Other statistical significance was examined by unpaired two-tailed *t*-test. The relative protein gray-scale value and the parameters in tube formation assay were analyzed by ImageJ (RRID: SCR_003070).

REFERENCES

1. Czabotar PE, Lessene G, Strasser A, Adams JM. Control of apoptosis by the BCL-2 protein family: implications for physiology and therapy. Nat Rev Mol Cell Biol. 2014;15:49–63.
2. Delbridge AR, Grabow S, Strasser A, Vaux DL. Thirty years of BCL-2: translating cell death discoveries into novel cancer therapies. Nat Rev Cancer. 2016;16:99–109.
3. Tsujimoto Y, Finger LR, Yunis J, Nowell PC, Croce CM. Cloning of the chromosome breakpoint of neoplastic B cells with the t(14;18) chromosome translocation. Science. 1984;226:1097–9.
4. Fukuhara S, Rowley JD. Chromosome 14 translocations in non-Burkitt lymphomas. Int J Cancer. 1978;22:14–21.
5. Singh R, Letai A, Sarosiek K. Regulation of apoptosis in health and disease: the balancing act of BCL-2 family proteins. Nat Rev Mol Cell Biol. 2019;20:175–93.
6. Hata AN, Engelman JA, Faber AC. The BCL2 family: key mediators of the apoptotic response to targeted anticancer therapeutics. Cancer Disco. 2015;5:475–87.
7. Riedell PA, Smith SM. Double hit and double expressors in lymphoma: definition and treatment. Cancer. 2018;124:4622–32.
8. Merino D, Kelly GL, Lessene G, Wei AH, Roberts AW, Strasser A. BH3-mimetic drugs: blazing the trail for new cancer medicines. Cancer Cell. 2018;34:879–91.
9. Ashkenazi A, Fairbrother WJ, Leverson JD, Souers AJ. From basic apoptosis discoveries to advanced selective BCL-2 family inhibitors. Nat Rev Drug Discov. 2017;16:273–84.
10. Warren CFA, Wong-Brown MW, Bowden NA. BCL-2 family isoforms in apoptosis and cancer. Cell Death Dis. 2019;10:177.
11. Guillem V, Amat P, Collado M, Cervantes F, Alvarez-Larran A, Martinez J, et al. BCL2 gene polymorphisms and splicing variants in chronic myeloid leukemia. Leuk Res. 2015;39:1278–84.
12. Martinou JC, Youle RJ. Mitochondria in apoptosis: Bcl-2 family members and mitochondrial dynamics. Dev Cell. 2011;21:92–101.
13. Konermann S, Brigham MD, Trevino AE, Joung J, Abudayyeh OO, Barcena C, et al. Genome-scale transcriptional activation by an engineered CRISPR-Cas9 complex. Nature. 2015;517:583–8.
14. Harris AW, Pinkert CA, Crawford M, Langdon WY, Brinster RL, Adams JM. The E mu-myc transgenic mouse. A model for high-incidence spontaneous lymphoma and leukemia of early B cells. J Exp Med. 1988;167:353–71.
15. Souers AJ, Leverson JD, Boghaert ER, Ackler SL, Catron ND, Chen J, et al. ABT-199, a potent and selective BCL-2 inhibitor, achieves antitumor activity while sparing platelets. Nat Med. 2013;19:202–8.
16. Reed JC, Cuddy M, Slabiak T, Croce CM, Nowell PC. Oncogenic potential of bcl-2 demonstrated by gene transfer. Nature. 1988;336:259–61.
17. Iervolino A, Trisciuoglio D, Ribatti D, Candiloro A, Biroccio A, Zupi G, et al. Bcl-2 overexpression in human melanoma cells increases angiogenesis through VEGF mRNA stabilization and HIF-1-mediated transcriptional activity. FASEB J. 2002;16:1453–5.
18. Massaad CA, Portier BP, Taglialatela G. Inhibition of transcription factor activity by nuclear compartment-associated Bcl-2. J Biol Chem. 2004;279:54470–8.
19. Froesch BA, Aime-Sempe C, Leber B, Andrews D, Reed JC. Inhibition of p53 transcriptional activity by Bcl-2 requires its membrane-anchoring domain. J Biol Chem. 1999;274:6469–75.
20. Kawatani M, Uchi M, Simizu S, Osada H, Imoto M. Transmembrane domain of Bcl-2 is required for inhibition of ceramide synthesis, but not cytochrome c release in the pathway of inostamycin-induced apoptosis. Exp Cell Res. 2003;286:57–66.
21. Borner C, Martinou I, Mattmann C, Irmler M, Schaerer E, Martinou JC, et al. The protein bcl-2 alpha does not require membrane attachment, but two conserved domains to suppress apoptosis. J Cell Biol. 1994;126:1059–68.
22. Biroccio A, Candiloro A, Mottolese M, Sapora O, Albini A, Zupi G, et al. Bcl-2 overexpression and hypoxia synergistically act to modulate vascular endothelial growth factor expression and in vivo angiogenesis in a breast carcinoma line. FASEB J. 2000;14:652–60.
23. Nor JE, Christensen J, Mooney DJ, Polverini PJ. Vascular endothelial growth factor (VEGF)-mediated angiogenesis is associated with enhanced endothelial cell survival and induction of Bcl-2 expression. Am J Pathol. 1999;154:375–84.
24. Dias S, Shmelkov SV, Lam G, Rafii S. VEGF(165) promotes survival of leukemic cells by Hsp90-mediated induction of Bcl-2 expression and apoptosis inhibition. Blood. 2002;99:2532–40.
25. Kase S, He S, Sonoda S, Kitamura M, Spee C, Wawrousek E, et al. alphaB-crystallin regulation of angiogenesis by modulation of VEGF. Blood. 2010;115:3398–406.
26. Bohonowych JE, Gopal U, Isaacs JS. Hsp90 as a gatekeeper of tumor angiogenesis: clinical promise and potential pitfalls. J Oncol. 2010;2010:412985.
27. Ozawa K, Kondo T, Hori O, Kitao Y, Stern DM, Eisenmenger W, et al. Expression of the oxygen-regulated protein ORP150 accelerates wound healing by modulating intracellular VEGF transport. J Clin Investig. 2001;108:41–50.
28. Gengrinovitch S, Berman B, David G, Witte L, Neufeld G, Ron D. Glypican-1 is a VEGF165 binding proteoglycan that acts as an extracellular chaperone for VEGF165. J Biol Chem. 1999;274:10816–22.
29. Chavez A, Scheiman J, Vora S, Pruitt BW, Tuttle M, PRI E, et al. Highly efficient Cas9-mediated transcriptional programming. Nat Methods. 2015;12:326–8.
30. Chen M, Chen X, Li S, Pan X, Gong Y, Zheng J, et al. An epigenetic mechanism underlying chromosome 17p deletion-driven tumorigenesis. Cancer Discov. 2021;11:194–207.
31. Zhang Q, Zhao L, Yang Y, Li S, Liu Y, Chen C. Mosaic loss of chromosome Y promotes leukemogenesis and clonal hematopoiesis. JCI Insight. 2022;7:153768.
32. DeCicco-Skinner KL, Henry GH, Cataisson C, Tabib T, Gwilliam JC, Watson NJ, et al. Endothelial cell tube formation assay for the in vitro study of angiogenesis. J Vis Exp. 2014;91:e51312.
33. Dobin A, Davis CA, Schlesinger F, Drenkow J, Zaleski C, Jha S, et al. STAR: ultrafast universal RNA-seq aligner. Bioinformatics. 2013;29:15–21.
34. Love MI, Huber W, Anders S. Moderated estimation of fold change and dispersion for RNA-seq data with DESeq2. Genome Biol. 2014;15:550.
35. Subramanian A, Tamayo P, Mootha VK, Mukherjee S, Ebert BL, Gillette MA, et al. Gene set enrichment analysis: a knowledge-based approach for interpreting genome-wide expression profiles. Proc Natl Acad Sci USA. 2005;102:15545–50.
36. Wei T, Simko V. R package 'corrplot': visualization of a correlation matrix (Version 0.92) 2021. https://github.com/taiyun/corrplot.

ACKNOWLEDGEMENTS

We thank Dr. Yuquan Wei for his generous support. We thank Dr. Ruizhan Tong and Dr. Yinglan Zhao for their technical assistance. We thank Dr. Jianjun Li for his clinical assistance. We thank all the lab members in the Chen and Liu laboratory for their insightful advice and kindly support. The results published here are in whole or part based upon data generated by the TCGA Research Network: https://www.cancer.gov/tcga. This work was supported by the National Natural Science Foundation of China (grants 82130007, 81670182, and 82073221), the National Key R&D Program of China (grants 2017YFA0505600 and 2018YFC2000305), the Sichuan Science and Technology Program (grants 2018JZ0077), and the 1.3.5 Project for Disciplines of Excellence, West China Hospital, Sichuan University (grants ZYJC21009 and ZYYC20007).

AUTHOR CONTRIBUTIONS

YL, XH, and LZ designed this study, XH, BW, SL, XW, PC carried out the experiments, LZ performed bioinformatics analyses, XH and LZ prepared and assembled the figure. PL and JX provide clinical samples and analyzed data. YL, CC, TN, and LD supervised the study and analyzed data. XH, LZ, and YL wrote the manuscript.

COMPETING INTERESTS

The authors declare no competing interests.

ADDITIONAL INFORMATION

Supplementary information The online version contains supplementary material available at https://doi.org/10.1038/s41388-022-02372-0.

Correspondence and requests for materials should be addressed to Lunzhi Dai or Yu Liu.